



Influence Rule of Projectile Density on the Characteristics of High-Speed Water-Entry Cavity

B. Hao^{1,2}, B. Yang^{1†}, C. J. Du³, H. Dai¹ and L. W. Liu¹

¹ School of Mechanical Engineering and Automation, Northeastern University, Shenyang110819, China

² School of Control Engineering, Northeastern University at Qinhuangdao, Qinhuangdao066004, China

³ Heilongjiang North Tool Co., Ltd, Mudanjiang157000, China

†Corresponding Author Email: yang95921b@163.com

(Received May 15, 2022; accepted July 7, 2022)

ABSTRACT

There has been much recent research on high-speed projectiles entering water, but research on the selection of the material for supercavitating projectiles is limited. Some important properties of such projectiles—mass and moment of inertia, for example—are related to the material density, so the projectile's density has an important effect on the performance of the supercavitating projectile. This study, using Ansys fluent 19.0 simulation software, studied the details of water entry of four high-speed projectiles of the same shape but made of different materials: aluminum (2.7 g/cm³), steel (7.85 g/cm³), brass (8.5 g/cm³), and tungsten alloy (17.5 g/cm³). The cavity shape, ballistic and hydrodynamic characteristics, and cavity flow field characteristics of projectiles with different densities were analyzed for a water-entry velocity of 600 m/s. The results show that within 3 ms, the velocity of a projectile with a density of 2.7 g/cm³ drops to 171.8 m/s, and the velocity of a projectile with a density of 17.5 g/cm³ drops to 433.1 m/s. Increasing the density of the projectile evidently reduces the deceleration of the projectile. The drag coefficient depends, primarily on the size and shape of the projectile, only slightly on its density. Just after water-entry time, the higher the density of the projectile, the faster the expansion of its cavity wall. As time after water entry increases, the expansion velocity of the cavity wall gradually decreases. The simulation results show that the projectile head experiences the greatest pressure, producing a sharp peak, at the moment when it touches the water surface. During the flow stabilization phase, the lower the density of the projectile, the lower the pressure on the head of the projectile. The results of this study will help to guide the selection of material for supercavitating projectiles.

Keywords: Supercavitating; Underwater projectile; Cavity shape; Density; Water-Entry.

NOMENCLATURE

A_0	projectile maximum cross-sectional area	R_B	gas-core radius in the Rayleigh equation
a	constant	S	invariant measure of shear strain rate
C_d	drag coefficient	s	projectile displacement
D	projectile main body diameter	T	temperature
d	projectile head diameter	t	time
F_l	blending function	u_i	velocity component in the direction i
F_{cond}	empirical constant	u_j	velocity component in the direction j
F_d	force of resistance on the projectile head	v	projectile velocity
F_{vap}	empirical constant	x_f, x_s	displacement of the fluid and solid
H	projectile length	x_i	distance in the direction i
h	axial length of the conical part of the projectile	x_j	distance in the direction j
(I_{xx}, I_{yy}, I_{zz})	moment of inertia	α_{nuc}	volume fraction of non-condensable gas
k	turbulent kinetic energy	β', β	constant
l	closest distance of a node in the flow field to the wall	σ_k, σ_ω	constant
n	direction vector	ϕ_l, ϕ_a, ϕ_v	volume fraction of water, air and water vapor phases
P	turbulent kinetic energy term due to	μ	dynamic viscosity
		μ_t	turbulence viscosity coefficient
		ρ	projectile density
		ρ_l, ρ_a, ρ_v	density of water, air, and water vapor

	velocity gradient		phases
$(P_{kb}, P_{\omega b})$	turbulent kinetic energy term due to buoyancy	ρ_m	mixed-phase density
P_v	pressure inside the water vapor	τ	stress
p	pressure	ν	kinematic viscosity
q	heat flow	ω	turbulence frequency

1. INTRODUCTION

For a liquid at a certain temperature, the formation of a gas phase pocket within it due to a reduction in pressure is called cavitation. When an underwater projectile travels at a sufficiently high speed, the surrounding pressure drops sharply, the extent of the low-pressure area continuously expands, and the cavitation area continues to develop until finally the length of the cavity exceeds the length of the projectile, so that the formed cavity can wrap around most or all of the projectile. This phenomenon is called supercavitation. When a projectile moving at high speed in water reaches a supercavitation state, the frictional resistance on its surface is greatly reduced, by up to 90%. This increases the speed of the projectile in the water and increases its underwater range, thereby increasing its lethality.

In recent years, supercavitation techniques have been applied to achieve significant drag reduction on high-speed underwater vehicles. It has had important strategic significance for underwater special combat projectiles such as high-speed torpedoes, submarine-launched missiles, and anti-torpedo weapons. Researchers have expended much effort on supercavitating weapons (Choi *et al.* 2005). In the early 1970s, the Soviet Union used supercavitation technology to develop the first generation of "Storm" supercavitating torpedoes, with maximum speeds reaching 100 m/s. Based on the principle of independent expansion, Logvinovich *et al.* (1973) solved the cavitation shape in water, and took into account that the radius of each cavitation section as a function of time is related to the size, velocity, and resistance of the moving body, and to the pressure of the distant flow field. They provided a theoretical basis for subsequent studies of cavity shape. Lee *et al.* (1997) used the energy equation to find that when a ball enters the water at a high speed, the cavity first closes in front and then the surface closes. If the ball enters the water at a lower speed, the cavity closes in the opposite way. Based on this work, a method of theoretical analysis for the shape change of cavities has been provided. Based on the Rayleigh-Besant problem, Yao *et al.* (2014) created a theoretical model to represent the evolution of the cavity shape, and concluded that up to a certain penetration distance, the square of the maximum cavity radius depends linearly on the square of the impact velocity of the projectile. Aristoff *et al.* (2009, 2010) conducted experimental and numerical studies on the vertical water entry of lightweight spheres, and described the sphere dynamics process and the effect of the decay of sphere velocity. Jafarian and Pishavar (2016) studied the effects of the cavitator head and the flow velocity on the cavity; the results showed that a sharper cavitator head leads to smaller cavity.

Based on previous studies on supercavitation, many researchers in this field began to study the influence of the physical parameters of projectiles on the shape of the cavity. May (1952) had studied the phenomenon of a moving body entering the water vertically, and analyzed the influence of the velocity and head shape of the moving body on the formation, development, and closed property of the cavity in the water. Bodily *et al.* (2014) conducted a low-speed (3 m/s) vertical water-entry test of a rotating body, and investigated the effects of head shape and surface characteristics on water-entry impact and ballistic deflection. Forouzani *et al.* (2018) investigated the effects of projectile mass, cavitator diameter and length on the performance of high-speed supercavitating projectiles. Shi *et al.* (2019) investigated the effects of cavitator shape, impact velocity and impact angle on the cavity after the projectile entered water, and found that as the impact velocity increases, the cavity is gradually elongated.

Previous reports primarily discussed the effects of water-entry velocity, cavitator shape, and water-entry angle on the water-entry performance of supercavitating projectiles, but there has been a lack of systematic and in-depth research on a related factor, density. In studying the problem of torpedo failure, Gilbarg and Anderson (1948) experimentally analyzed how different factors depend on the water-entry cavity, and found that air density has a significant effect on the closing time of the cavity surface near the point of water entry. In recent years, some researchers have studied the cavity changes of projectiles when the projectiles navigate in regions of different liquid density (Fan *et al.* 2019). Some researchers have also proved that density is an important factor in materials and has a certain influence on the range and power of projectile, both experimentally and theoretically (Forouzani *et al.* 2018; Sorensen *et al.* 2008; Wang *et al.* 2020; Zhang *et al.* 2021). It seems clear that studying the effect of projectile density on the performance of supercavitating projectiles will increase scientific understanding of high-speed entry into water. Therefore, in order to augment understanding in this area, we study the effect of different projectile densities on the water-entry process of supercavitating projectiles.

At present, most researchers use computer simulation software to study the process of high-speed projectile entering water. Through numerical simulation, the influences of various characteristics of the projectile during water entry can be analyzed. To numerically simulate the water entry process of a moving body Gaudet (1998) applied computer simulation software combined with theoretical analysis, setting the parameters of the fluid, and then simulating the process. The parameters of the cavity

flow field and the resistance of the moving body calculated from the computer software were close to the theoretical results. Gao *et al.* (2019) used CFD software to numerically simulate the oblique entry of a projectile into water. The study showed that parameters such as projectile shape and length affect the deceleration after entry. Nair and Bhattacharyya (2018) applied CFD software to simulate the water inflow process of a rigid axisymmetric body, and reproduced the projectile water-entry process well. Akbari *et al.* (2021) used CFD software to study the stability of cylindrical projectiles when they enter water obliquely in the presence of air, water, and vapor, and analyzed the effects of the projectile length/diameter ratio and water inlet angle on the internal stability of cavity.

Forouzani *et al.* (2018) studied the effect of the mass of the projectile on the cavity phenomenon and found that with an increase of projectile mass and corresponding increase of initial kinetic energy, the axial cavity size increased. However, there is a lack of in-depth research on the cavity morphology, ballistic and hydrodynamic characteristics, and cavity flow field characteristics of supercavitating projectiles entering water.

In order to achieve the goal of this study, the CFD software Ansys fluent 19.0 was used to simulate the water entry of four projectiles of the same size but different densities entering the water vertically with an initial velocity of 600 m/s. This study used the Reynolds time-averaged Navier-Stokes equation, and applied the volume-of-fluid (VOF) multiphase flow model, the SST k- ω model, and the Schnerr-Sauer cavitation model, combined 6- degrees-of-freedom (DOF) dynamic grid technology. Finally, the rules governing the influence of the density of projectiles on the cavity shape, ballistic and hydrodynamic characteristics, and cavity flow field characteristics were analyzed. This study broadens the field of study in material selection for supercavitating projectiles. Combining the results of this study with previous experimental results will yield a more detailed description of the density factors of high-velocity projectiles.

2. MATHEMATICAL MODEL AND NUMERICAL CALCULATION

2.1 Basic Governing Equations

2.1.1 Continuity equation

This study is based on the finite volume method. It combines the continuity equation and momentum equation, and selects the VOF multiphase flow model to numerically simulate the cavity shape, ballistic and hydrodynamic characteristics and cavity flow field characteristics of projectiles with different densities. Through the flow of each phase among the gas, the vapor, and the liquid, the control equation for the problem is established. Its volume fraction relationship in the flow field is

$$\varphi_l + \varphi_a + \varphi_v = 1 \quad (1)$$

Where φ_l , φ_a , and φ_v are the volume fractions of water phase, air phase, and water vapor phase, respectively.

The density expression for the mixed phase is

$$\rho_m = \varphi_l \rho_l + \varphi_a \rho_a + \varphi_v \rho_v \quad (2)$$

Where ρ_l , ρ_a , and ρ_v are the densities of the water phase, air phase, and water vapor phase respectively.

The continuity equation and momentum equation for the mixed phase are as follows:

Continuity equation:

$$\frac{\partial \rho_m}{\partial t} + \frac{\partial (\rho_m u_i)}{x_i} = 0 \quad (3)$$

Momentum equation:

$$\frac{\partial (\rho_m u_i)}{\partial t} + \frac{\partial (\rho_m u_i u_j)}{x_j} = - \frac{\partial p}{\partial x_i} + \frac{\partial}{\partial x_i} \left[\mu \left(\frac{\partial u_i}{\partial x_j} + \frac{\partial u_j}{\partial x_i} \right) \right] \quad (4)$$

In these equations, μ is the mixed-phase dynamic viscosity, ρ_m is the mixed phase density, u_i is the velocity component in the direction I , u_j is the velocity component in the direction j , x_i is distance in the direction i , x_j is distance in the direction j , and p is the far-field pressure.

2.1.2 Turbulence Model

The Reynolds time-averaged numerical simulation method refers to the use of time-averaged and pulsating quantities to describe the turbulence model. This can avoid the direct solution of the unsteady Navier-Stokes equation, thereby reducing the computational complexity of the computer. In this paper, the Reynolds time-averaged numerical simulation method is used for the simulation of the high-speed projectile into water. The SST k- ω turbulent model, used in this study, combines the advantages of the k- ϵ and k- ω turbulence models, and has significant advantages for predicting near-wall flow and swirl (Menter 2003), and the calculation accuracy of the high-speed projectile entering the water is improved. The specific expressions for the turbulent kinetic energy and turbulent frequency of the SST k- ω turbulence model are as follows:

$$\frac{\partial (\rho_m k)}{\partial t} + \frac{\partial (\rho_m u_j k)}{\partial x_j} = \frac{\partial}{\partial x_j} \left[(\mu + \sigma_k \mu_t) \frac{\partial k}{\partial x_j} \right] - \beta' \rho_m \omega k + P + P_{kb} \quad (5)$$

$$\frac{\partial (\rho_m \omega)}{\partial t} + \frac{\partial (\rho_m u_j \omega)}{\partial x_j} = \frac{\partial}{\partial x_j} \left[(\mu + \sigma_\omega \mu_t) \frac{\partial \omega}{\partial x_j} \right] - \beta \rho_m \omega^2 + \alpha \frac{\omega}{k} P + 2 \rho_m (1 - F_1) \sigma_\omega \frac{1}{\omega} \frac{\partial k}{\partial x_j} \frac{\partial \omega}{\partial x_j} + P_{\omega b} \quad (6)$$

Where k is the turbulent kinetic energy, ω is the turbulence frequency, μ is the dynamic viscosity coefficient of fluid, μ_t is the turbulence viscosity coefficient, P is the turbulent kinetic energy term due to velocity gradient, P_{kb} and $P_{\omega b}$ are the turbulent kinetic energy term due to buoyancy, β' , β , σ_k, σ_ω are constants, ρ_m is the mixed-phase density, x_i is the distance in the direction i , x_j is the distance in the direction j , F_1 is the blending function. The specific expression for μ_t is

$$\mu_t = \frac{\rho_m a k}{\max(a\omega, SF_1)} \quad (7)$$

Where a is the constant, $S = \sqrt{2W_{ij} \cdot W_{ij}}$ is the invariant measure of shear strain rate, $F_1 = \tanh(\arg_2^2)$ is the blending function, where W_{ij} and \arg_2 are specific expressions as follows:

$$w_{ij} = \frac{1}{2} \left(\frac{\partial u_i}{\partial x_j} - \frac{\partial u_j}{\partial x_i} \right) \quad (8)$$

$$\arg_2 = \max \left(\frac{2\sqrt{k}}{\beta'\omega l}, \frac{500\nu}{l^2\omega} \right) \quad (9)$$

In Eq. (9), k is the turbulent kinetic energy, ω is the turbulence frequency, β is a constant, l is the closest distance of a node in the flow field to the wall, and ν is the kinematic viscosity coefficient of fluid.

2.1.3 Cavitation model

In this study, in order to solve the cavitation problem of projectiles with different densities in underwater motion, the model proposed by Schnerr and Sauer was used for simulation; it captures the phase transition from water to water vapor (Schnerr and Sauer 2001). The governing equation is

$$\frac{\partial \varphi_v}{\partial t} + \frac{\partial}{\partial x_i} (\varphi_v u_i) = F_{vap} \frac{2\alpha_{nuc}(1-\varphi_v)\rho_v}{R_B} \sqrt{\frac{2}{3} \frac{P_v - P}{\rho_l}} - F_{cond} \frac{3\varphi_v \rho_v}{R_B} \sqrt{\frac{2}{3} \frac{P - P_v}{\rho_l}} \quad (10)$$

where $F_{vap}=50$ and $F_{cond}=0.001$ are empirical constant, $\alpha_{nuc}=5 \times 10^{-4}$ is the volume fraction of non-condensable gas, $R_B=1 \times 10^{-6} m$ is the gas core radius in the Rayleigh equation. The value range of these parameters are based on the literature (Meng *et al.* 2019), P_v is the pressure inside the water vapor, ρ_l is the density of water, ρ_v is the density of water vapor.

2.1.4 Fluid-Structure Interaction Equation

The fluid-structure interaction follows the most basic continuity principle, so variables such as fluid and solid stress, displacement, heat flow, and temperature are the same on both sides of the contact surface between projectile surface and water. The equations are

$$\begin{cases} \tau_f n_f = \tau_s n_s \\ x_f = x_s \\ q_f = q_s \\ T_f = T_s \end{cases} \quad (11)$$

Where τ is the stress, x is the displacement, q is the heat flow, and T is the temperature. The subscript f stands for fluid, the subscript s for solid.

2.2 Computation Model

In order to study the influence of projectile density on the characteristics of high-speed water-entry cavitation, and to improve the calculation speed and reduce the calculation time, a three-dimensional model was applied in this study to numerically simulate projectile vertical water entry. For the water-entry analysis of projectiles with different densities, a projectile of 5.8 mm caliber was selected as the model for calculation. High-speed projectiles in the study have the same shape, size, and water-entry speed (600 m/s), and enter the water vertically, but they are made of different materials and, accordingly, have different densities and masses. The overall dimensions of a projectile are shown in Fig.1. The projectile head is a truncated cone, the tail is a cylinder, the total length H of the projectile is 30 mm, the diameter d of the head is 2.6 mm, and the axial length h of the conical part is 16.5 mm. For the selection of projectile materials, four widely used bullet materials are selected as the research objects. Arranged from low to high density, they are aluminum (2.7 g/cm³), steel (7.85 g/cm³), brass (8.5 g/cm³) and tungsten alloy (17.5 g/cm³). The water entry of these four projectiles was analyzed, and the influence of cavity shape, ballistics, hydrodynamics, and cavitation flow field of projectiles entering the water were studied. The physical properties of the projectiles of four different densities are shown in Table 1.

2.3 Computational Domain and Boundary Conditions

Figure 2 shows the computational domain for the $z = 0$ plane. The length of the computational domain is 2059 mm, its diameter is 580 mm, the height of the air domain of the flow field is 1740 mm, the depth of

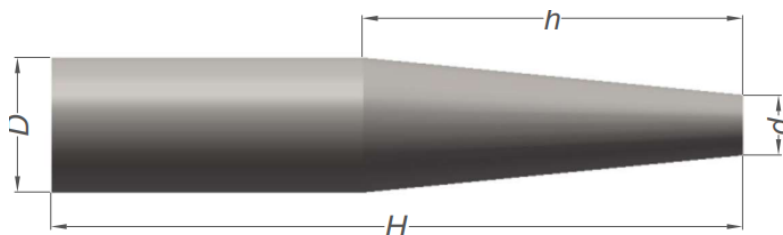


Fig. 1. Projectile model.

Table 1 Physical properties of four kinds of projectiles with different densities

Material	Density (g/cm ³)	Mass (g)	Moment of inertia (g·cm ²)		
			I _{xx}	I _{yy}	I _{zz}
aluminum	2.70	1.610	5.811	95.592	95.592
steel	7.85	4.681	16.896	277.924	277.924
brass	8.50	5.069	18.295	300.936	300.936
tungsten alloy	17.50	10.436	37.666	619.575	619.575

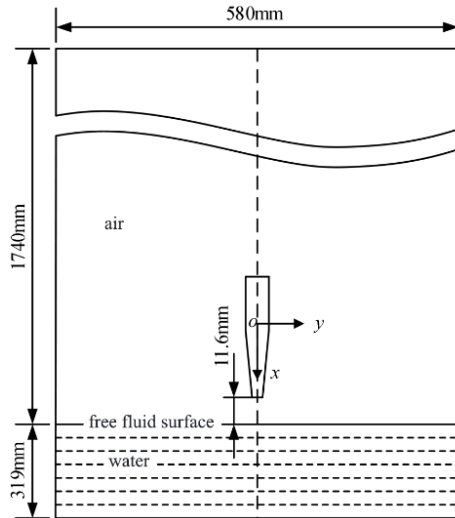


Fig. 2. Schematic diagram of computational domain.

the water domain is 319 mm. The direction of gravity is along the positive direction of the x-axis. At the initial moment, the projectile is coaxial with the computational domain, the initial velocity of the projectile is 600 m/s, the position of the projectile mass center is chosen as the origin of the coordinates, and the distance between the center of the projectile head and the free liquid surface is 11.6 mm. The top, bottom and both sides of the computational domain are pressure port boundaries, the axis of the

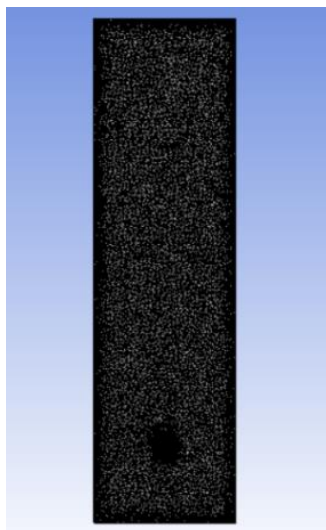
computational domain is an axisymmetric boundary, and the surface of the projectile is a wall condition. In this study, a tetrahedral structured grid is used. As shown in the Fig. 3, in order to ensure the accuracy of the force on the projectile and its state of motion, as well as the accuracy of the cavitation shape, the grid of the space immediately around the projectile is refined.

2.4 Numerical Method

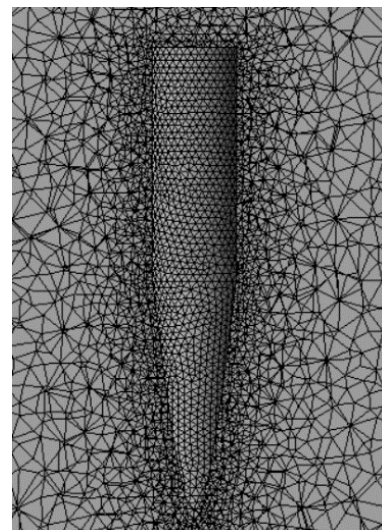
Based on the finite volume method of the VOF multiphase flow model, the discrete method of the fluid governing equations in time and space was selected in this study. The coupled algorithm was applied to solve the momentum equation and the continuity equation simultaneously, and the coupling relationship between the velocity field and the pressure field was established. The spatial dispersion of the pressure field adopted the PRESTO format, and the gradient solution adopts the least square method. The dissipative term and the turbulence and momentum equations all adopted the second-order upwind style. Considering factors such as grid scale and speed of motion, the calculation time step was determined, and the projectile motion process and grid update were realized through moving grid technology.

2.5 Verification of the Numerical Method

In order to verify the accuracy of the numerical method, numerical simulation was applied to the vertical water entry of the flat-head projectile model



(a) Global grid.



(b) Local grid.

Fig. 3. Grids of computing domain.

in the literature (Guo 2012). Numerical simulation was performed according to the size of the experimental projectile model, and the simulation results were compared with published simulation results (Guo 2012). In this comparison example, the diameter of the projectile is 12.65 mm, its length is 38.1 mm, and its initial water-entry speed is 498.1 m/s. By analyzing calculated results, we obtained the relationship between the velocity of the projectile and its depth of penetration into the water with time, as shown in Fig. 4. It can be seen from this figure that the rate of change of the projectile's velocity (its deceleration) gradually becomes smaller. This is due to the large fluid resistance experienced by the projectile during the initial phase of entry into the water and the subsequent decrease of this resistance. As the resistance decreases, the velocity decay decreases, and the rate of increase in the depth of penetration also decreases. The curves of the numerical simulation results in this study are quite close to those determined experimentally (Guo 2012). This agreement confirms the accuracy of the numerical simulation method of this study.

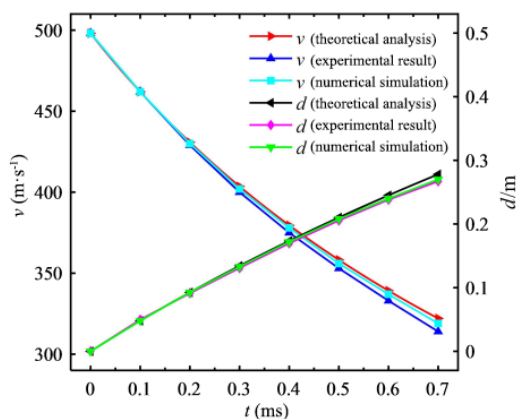


Fig. 4. Comparison of experimental and numerically simulated results for speed and depth of penetration.

3. COMPUTATIONAL RESULTS AND ANALYSIS

In the presence of the three phases of air, water, and water vapor, the projectiles, as noted above, have the same shape, size and water-entry speed, but they are made of four materials of different density: aluminum, steel, brass, and tungsten alloy. Through numerical simulation, the effect of density on the stability of projectiles entering water was studied. Because of the super-cavitation formed while the projectile entering the water at high speed, the resistance of the projectile can be reduced by more than 90%, thereby increasing the range and power of the projectile. Studying the cavity shape, ballistic and hydrodynamic characteristics, and cavity flow... These can well reflect the motion state of the projectile underwater. By analyzing these parameters, the stability of projectile entering water can be well judged.

3.1 Analysis of Cavity Shape in Water Entry

Figure 5 shows the water phase volume fraction nephogram of projectiles with different densities. During the first 0.2 ms, the sizes of the cavities generated by the four different projectiles entering the water are almost the same (see Fig. 5(a)). As the time increases to 0.6ms, it can be seen from Fig. 5(b) that the projectile with a density of 2.7 g/cm³ produces the smallest axial size of the cavitation, the projectiles with densities of 7.85 and 8.5 g/cm³ produce substantially the same size of cavity, and the projectile with a density of 17.5 g/cm³ produces the largest cavity. When the time reaches 1 ms, the differences in the axial sizes of the cavities generated by projectiles with different densities becomes more and more obvious (see Fig. 5(c)). This is because, for the same size of the projectile, the greater the density of the projectile, the greater its own mass, which helps to increase the axial size of the cavity, thereby improving the stability of the projectile in water.

Figure 6 compares the cavity shapes for the four projectiles with different densities at 0.2 ms after entering the water. At this moment after entry, the axial dimension of the cavity for a projectile with a density of 2.7 g/cm³ is about 130 mm. As the density increases, the axial dimension of the cavity also increases. At the highest studied density, 17.5 g/cm³, the axial dimension of the cavity of the projectile is the greatest, 136.5 mm. At a depth of 128 mm, the cavity radius for the projectile with a density of 2.7 g/cm³ is 2.3 mm, which is about 1.4 mm less than for the higher-density projectiles. But at the fluid-solid interface, the cavity radius of the projectiles for all four densities is 2 mm. This is because the projectiles are all the same size and have the same wetted area in contact with the water surface. Therefore, the cavity radius generated by the impact on the water surface is initially the same. But at the same depth of water, as the density increases, the increase of mass causes the impact force of the water entry and therefore the cavity radius to increase.

Figure 7 shows a comparison of the cavity shapes of projectiles with four different densities when the projectile underwater depth is $3H$. As shown in the figure, at the outward development stage of the cavity, the cavity radius gradually increases from the projectile head to the free liquid surface. When the depth in the water is 60.005 mm, the cavity radius of the projectile with a density of 2.7 g/cm³ is 8.52 mm. As the density increases, the cavity radius of the projectile decreases gradually. For a density of 17.5 g/cm³, the cavity radius of the projectile drops to 8.36 mm. In short, the greater the projectile density, the less the radius of the cavity. It can also be seen in Fig. 7 that the increase in height of the water surface caused by projectiles of different densities is about 10 mm. This is because projectiles of different densities experience little difference in resistance for a given speed, indicating that fluid particles near the projectile initially receive approximately the same amount of energy.

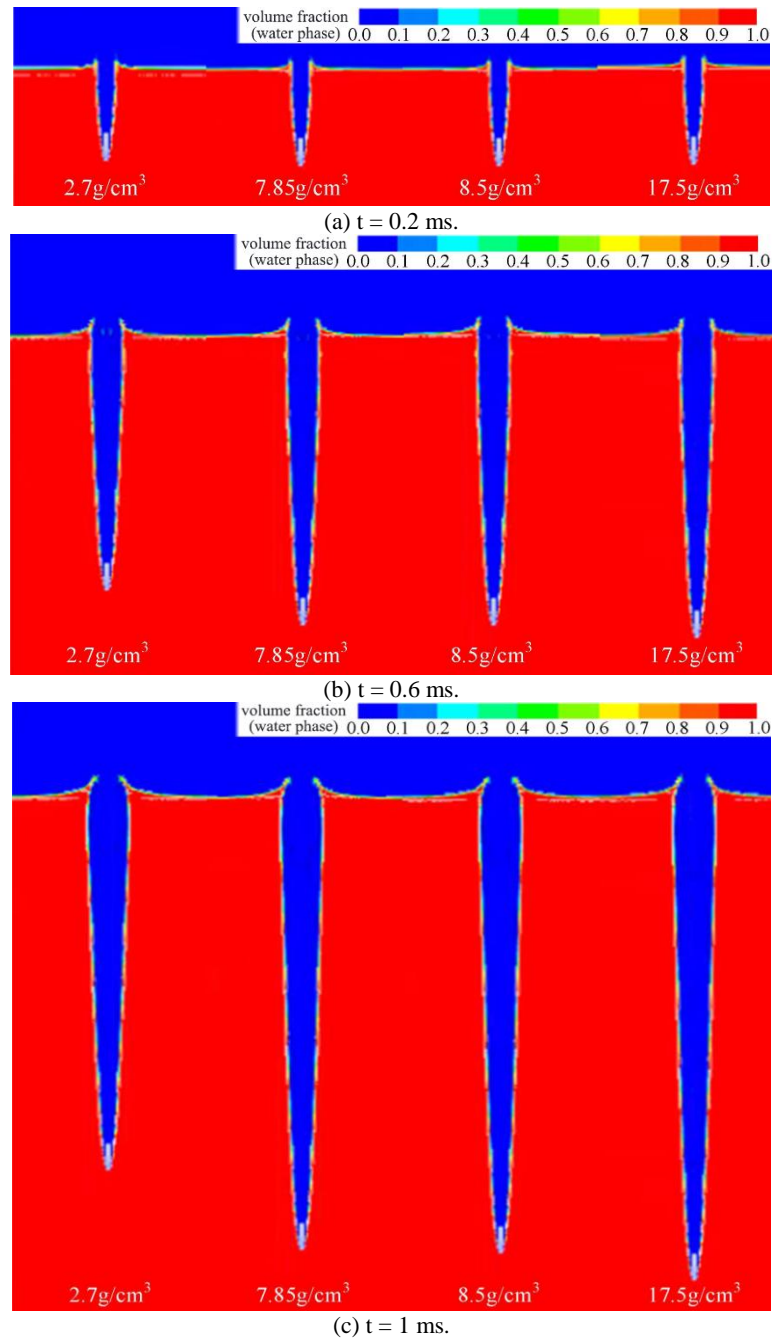


Fig. 5. Cavitation cavities for the first millisecond after projectile entry into the water.

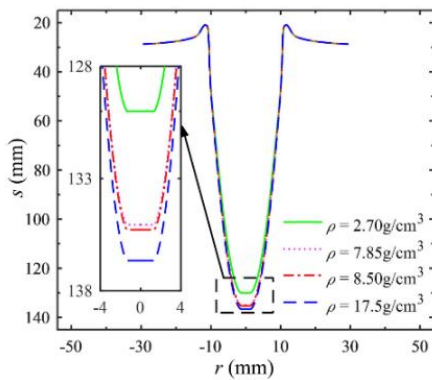


Fig. 6. Comparison of the cavity shapes at 0.2 ms.

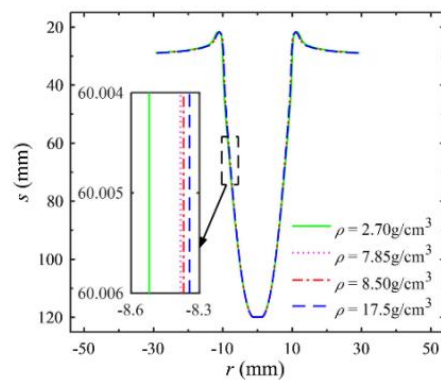


Fig.7. Comparison of cavity shapes when the penetration depth into the water is 3H.

Table 2 Velocity decay rate (deceleration) of projectile of different density in the first 3 ms

Density (g/cm ³)	Initial velocity (m s ⁻¹)	Final velocity (m s ⁻¹)	Time (ms)	Average deceleration (m s ⁻²)
2.70	600	171.8	3	142.7
7.85	600	322.8	3	92.4
8.50	600	334.6	3	88.5
17.50	600	433.1	3	55.6

3.2 Analysis of Water Entry Ballistics and Hydrodynamic Characteristics

Figure 8 shows the time dependence of velocities for projectiles of different densities. Table 2 shows the velocity decay rate (deceleration) of the projectiles for different densities. As can be seen from Fig. 8, the speed drops significantly just after the projectile enters the water, and drops more significantly for lower density. The velocity of the projectile with a density of 2.7 g/cm³ drops from 600 to 171.8 m/s in 3 ms. For a projectile density of 17.5 g/cm³, the velocity drops to 433.1 m/s. From Fig. 8, it can be seen that the deceleration diminishes over time. This behavior is attributable to the law of frictional force in water, given by

$$F_d = \frac{1}{2} \rho_l v^2 A_0 C_d \quad (12)$$

Where ρ_l is the density of the water, v is the projectile velocity, A_0 is the projectile's maximum cross-sectional area, and C_d is the drag coefficient.

As the projectile speed decreases, the resistance it receives decreases, so the deceleration diminishes. Since, for a given force, the deceleration is inversely proportional to mass, there is a big difference in decelerations for projectiles of different densities. At the same moment, therefore, the velocity of the projectile with a density of 17.5 g/cm³ is significantly greater than that of the other projectiles. The projectile with a density of 17.5 g/cm³ has an average deceleration over the first 3 ms of 55.6 m s⁻², while for the projectile with a density of 2.7 g/cm³, the same quantity is 142.7 m s⁻². Increasing the density of the projectile can effectively diminish its deceleration.

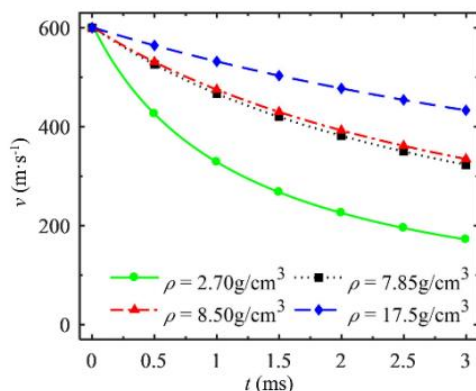


Fig. 8. Time dependence of velocities for projectiles of different densities.

Figure 9 shows displacements as functions of time for projectiles of different densities. After 3 ms, the low-density projectile (2.7 g/cm³) has penetrated the water to a depth of about 0.95 m. The projectiles of densities 7.85 and 8.5 g/cm³ at the same time have penetrated to depths that are, respectively, 36.8% and 38.9% greater. For the highest density projectile (17.5 g/cm³) the penetration at this time is 1.55 m, significantly greater than for the lower-density projectiles. The use of high-density projectiles can significantly increase the effective range of underwater projectiles. Another study has asserted that greater projectile mass will increase the underwater range of a projectile (Forouzani 2018). However, the change of density affects the projectile mass, so this study further explores the effect of density on the projectile range by combining previous studies. In summary, in the design of weapons in the form of supercavitating high-speed projectiles, the selection of high-density metallic materials has practical significance for improving the effective range and lethality of the projectiles.

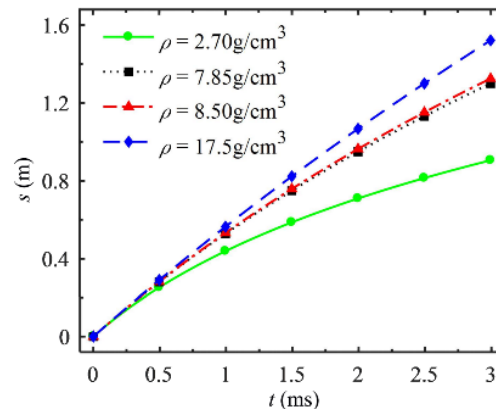


Fig. 9. Variation curve of projectile displacement.

Figure 10 shows how the projectile drag coefficients vary with time for different densities during the first 3 ms after water entry. Fig.10(b) is an enlarged view of the first 0.05 ms, and Fig.10(c) is an enlarged view for the time span 1.0-1.2 ms, with stable cavity flow. It can be seen from Figs. 10(a) and (b) that the initial drag coefficients are the same for projectiles with different density. There is an initial momentary drag coefficient peak of about 0.82. After the cavitation flow is stable, the drag coefficient drops to 0.18 and remains nearly constant. Fig.10(c) shows that around 1 ms, after the projectiles enter a stable flow stage, the drag coefficient of the low-density (2.7 g/cm³) projectile is 0.1697, and is slightly greater for higher-

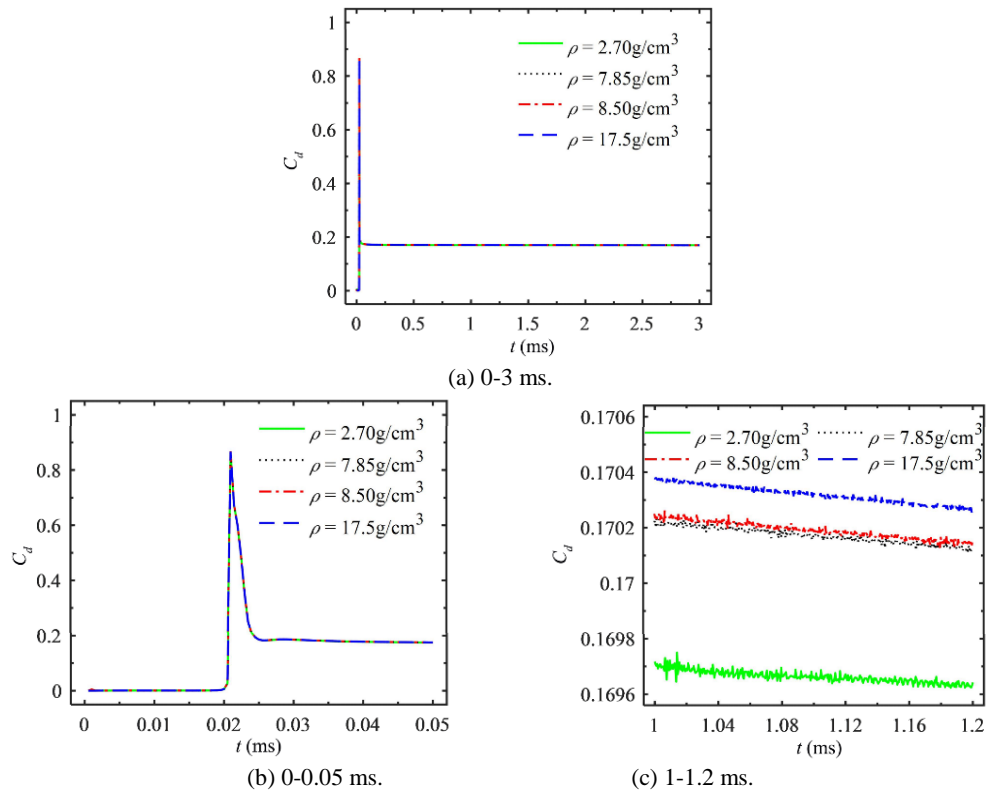


Fig. 10. Drag coefficients as functions of time for various projectiles. Panels (b) and (c) are expanded sections of Panel (a).

density projectiles—greater by 0.0005, 0.00052, 0.0007, respectively, for projectile densities 7.85 g/cm³, 8.5 g/cm³, 17.5 g/cm³. This is because the higher the projectile density, the faster the projectile velocity, the greater the drag, resulting in an increase in the drag coefficient. It can be seen from Fig. 10 that there is a small difference in the drag coefficient values of projectiles of different densities, indicating that the projectile density has little influence on the drag coefficient.

3.3 Analysis of Cavity Flow Field Characteristics in Water Entry

Figure 11 shows the maximum pressure at the head of projectiles with different densities as a function of time for the first 3 ms, with enlarged views for 0 to 0.1 ms and 1.0 to 1.2 ms (the latter being the stable stage of the cavity flow). When in air, the projectile head experiences a very small pressure, and, briefly, just after impact, a spike of pressure, reaching a peak value about 11,600 times atmospheric pressure. After the cavity flow is stabilized, the pressure drops very slowly. Within 0.024 ms after the water entry, the pressure dropped to 2000 times atmospheric pressure, about 82.6% less than the peak pressure upon entering the water. As can be seen in Fig. 11(c), at 1 ms, the pressure at the head of the projectile with a density of 2.7 g/cm³ is about 520 times atmospheric, and for the projectile with a density of 17.5 g/cm³ about 1400 times atmospheric. When the projectile contacts the free liquid surface, the pressure at its head is the largest. After entering the water and creating a cavity that wraps around the projectile, the pressure on the projectile drops rapidly

and become nearly flat (Shang 2013). For projectiles of different densities, the pressure peaks reached at their heads are almost the same. When the flow enters a stable stage, the less the density of the projectile, the less the projectile velocity, and the less the maximum pressure on its head.

Figure 12 depicts the velocity vectors of the cavity wall for the four densities of projectiles at 0.5 and 1.0 ms. For projectiles of different densities, the distribution of the velocity vector on the cavity wall is similar, with the cavity velocity decreasing from the projectile head to the free liquid surface. At 0.5 ms, the maximum expansion velocity of the cavity wall of the low-density projectile (2.7 g/cm³) is the smallest, 894 m/s. As the density increases, the expansion velocity of the cavity wall also increases. For a projectile density of 17.5 g/cm³, the expansion velocity of the cavity wall surface reaches a maximum of 1190 m/s. As the time advances to 1 ms, the maximum expansion velocity of the cavity wall of the low-density projectile (2.7 g/cm³) decreases by 23.2%. For projectiles with densities of 7.85 and 8.5 g/cm³, it decreases by 11.53% and 10.7%, respectively. For the highest-density projectile (17.5 g/cm³), the maximum expansion velocity of the cavitation wall decreases by only 5.9%. So, at the same time following water entry, increasing the density of the projectile increases the expansion speed of the cavity wall. At the same time, the higher the density of the projectile, the more slowly does the expansion rate of the cavity wall decrease, which indicates that the expansion process of the cavity wall is decelerating motion.

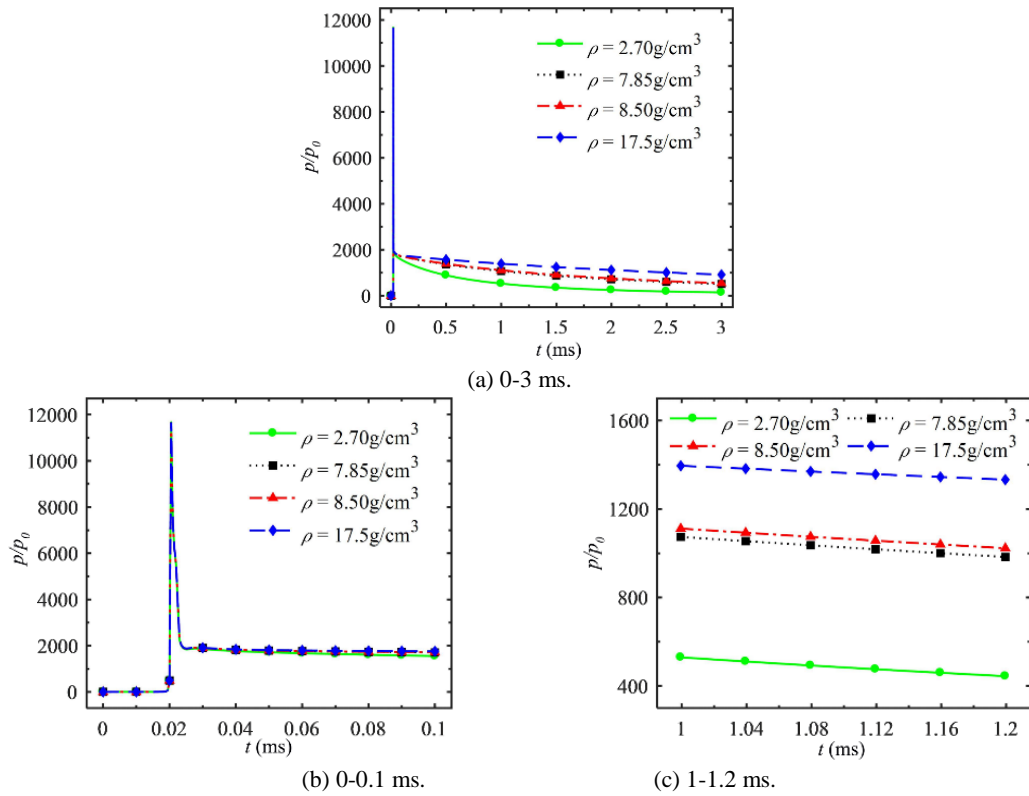


Fig. 11. Maximum pressure at projectile head as a functions of time for various projectiles. Panels (b) and (c) are expanded sections of Panel (a).

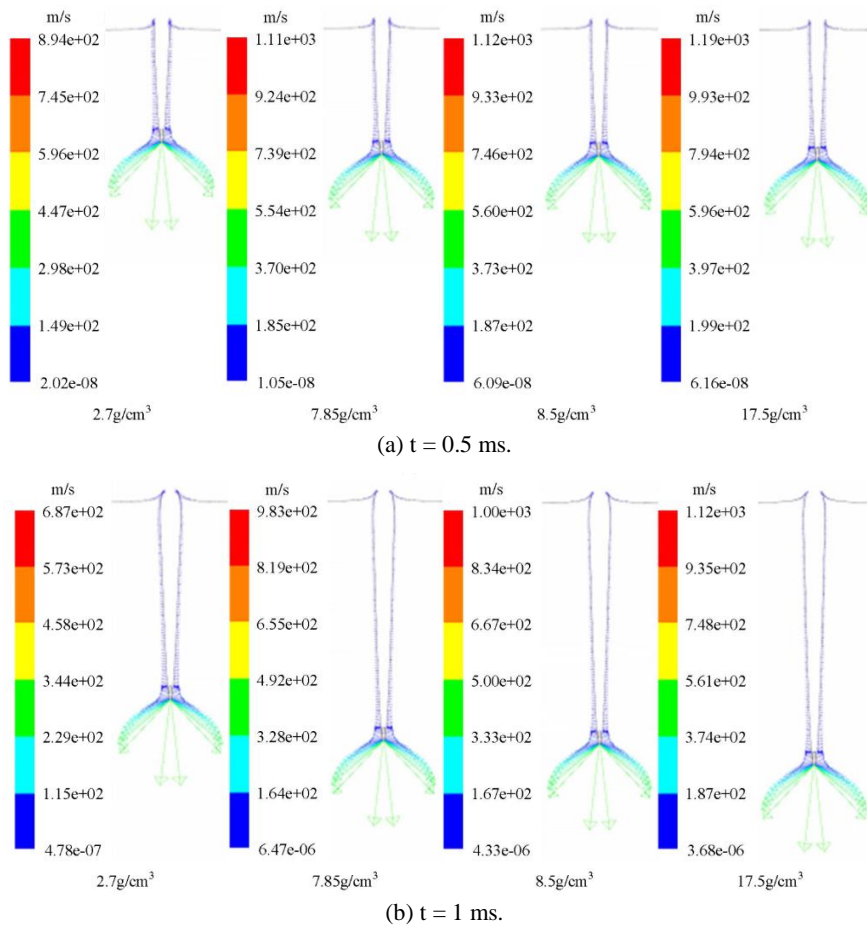


Fig. 12. Velocity vector diagrams at cavity wall.

4. CONCLUSION

In order to study the effect of projectile density (or, equivalently, of projectile mass) on the stability of projectiles entering water at high speed, simulations were carried out to explore the changing laws of cavity shape, ballistic characteristics, hydrodynamic characteristics, and cavity flow-field characteristics during vertical water entry of projectiles of the same shape but different densities. Four densities were chosen for study, those of aluminum (2.7 g/cm^3), steel (7.85 g/cm^3), brass (8.5 g/cm^3), and tungsten alloy (17.5 g/cm^3). An initial velocity of 600 m/s was used for all. The studies were carried out using CFD simulation software. The following results were obtained:

- (1) Following entry into the water, a projectile of greater density experiences less deceleration and more penetration depth.
- (2) Calculated drag coefficients are nearly the same for projectiles of the same shape and different densities
- (3) At a given time after water entry, projectiles of greater density have greater expansion velocity of the cavity wall and, correspondingly, less deceleration of that wall.
- (4) Pressure on the head of a projectile is greatest at the moment of impact with the water, and can reach 11,600 times atmospheric pressure. After the flow stabilization stage, pressure on the head is greater for greater projectile density and, for all projectiles, decreases slowly with time.

REFERENCES

- Akbari, M. A., J. Mohammadi and J. Fereidooni (2021). Stability of oblique water entry of cylindrical projectiles. *Journal of Applied Fluid Mechanics* 14(1), 301-314.
- Aristoff, J. M. and J. W. M. Bush (2009). Water entry of small hydrophobic spheres. *Journal of Fluid Mechanics* 619,45-78.
- Aristoff, J. M., T. T. Truscott, A. H. Techet and J. W. M. Bush (2010). The water entry of decelerating spheres. *Physics of Fluids* 625,135-165.
- Bodily, K. G., S. J. Carlson and T. T. Truscott (2014). The water entry of slender axisymmetric bodies. *Physics of Fluids* 26(7), 45-78.
- Choi, J. H., R. C. Penmetsa and R. V. Grandhi (2005). Shape optimization of the cavitator for a supercavitating torpedo. *Structural and Multidisciplinary Optimization* 29(2), 159-167.
- Fan, C. Y., Z. L. Li, B. C. Khoo and M. C. Du (2019). Supercavitation phenomenon research of projectiles passing through density change area. *Aip Advances* 9(4).
- Forouzani, H., B. Saranjam and R. Kamali (2018). A study on the motion of high-speed supercavitating projectiles. *Journal of Applied Fluid Mechanics* 11(6), 1727-1738.
- Gao, J. G., Z. H. Chen, Z. G. Huang, W. T. Wu and Y. J. Xiao (2019). Numerical investigations on the oblique water entry of high-speed projectiles. *Applied Mathematics and Computation* 362.
- Gaudet, S (1998). Numerical simulation of circular disks entering the free surface of a fluid. *Physics of Fluids* 10(10), 2489-2499.
- Gilbarg, D. and R. A. Anderson (1948). Influence of atmospheric pressure on the phenomena accompanying the entry of spheres into water. *Journal of Applied Physics* 19(2), 127-139.
- Guo, Z. T (2012). *Research on characteristics of projectile water entry and ballistic resistance of targets under different mediums*. Ph. D. thesis, Harbin Institute of Technology, Harbin, China.
- Jafarian, A. and A. Pischevar (2016). Numerical Simulation of Steady Supercavitating Flows. *Journal of Applied Fluid Mechanics* 9(6), 2981-2992.
- Lee, M., R. G. Longoria and D. E. Wilson (1997). Cavity dynamics in high-speed water entry. *Physics of Fluids* 9(03), 540-550.
- Logvinovich, G. V. (1973). *Hydrodynamics of flows with free boundaries*. Halsted Press.
- May, A. (1952). Vertical entry of missiles into water. *Journal of Applied Physics* 23(12), 1362-1372.
- Meng, Q. C., W. B. Yi., M. Y. Hu., Z. H. Zhang and J. B. Liu (2019). Study on Cavity Profile and Hydrodynamics of High-speed Vertical Water Entry of Projectile. *Shipbuilding of China* 60(03),12-26.
- Menter, F. R., M. Kuntz and R. Langtry (2003). Ten years of industrial experience with the SST turbulence model. *Turbulence Heat & Mass Transfer* 4, 625-632.
- Nair, V. V. and S. K. Bhattacharyya (2018). Water entry and exit of axisymmetric bodies by CFD approach. *Journal of Ocean Engineering and Science* 3(2),156-174.
- Schnerr, G. H. and J. Sauer (2001). Physical and numerical modeling of unsteady cavitation dynamics. *Fourth International Conference on Multiphase Flow* (Vol. 1).
- Shang, Z (2013). Numerical investigations of supercavitation around blunt bodies of submarine shape. *Applied Mathematical Modelling* 37(20-21), 8836-8845.
- Shi, Y., G. H. Wang and G. Pan (2019). Experimental study on cavity dynamics of projectile water entry with different physical parameters. *Physics of Fluids* 31(6).
- Sorensen, B. R., K. D. Kimsey and B. M. Love (2008). High-velocity impact of low-density projectiles on structural aluminum armor. *International Journal of Impact Engineering*

B. Hao *et al.* / *JAFM*, Vol. 15, No. 6, pp. 1901-1912, 2022.

35(12), 1808-1815.

Wang, X. F., J. B. Liu, B. Wu, D. F. Kong, J. R. Huang, X. Y. Xu and X. Bao (2020). Cratering for Impact of Hypervelocity Projectiles into Granite Targets within a Velocity Range of 1.91-3.99 km/s: Experiments and Analysis. *Applied Sciences-Basel*, 10(4).

Yao, E. R., H. R. Wang, L. Pan, X. B. Wang and R.

H. Woding (2014). Vertical water-entry of bullet-shaped projectiles. *Journal of Applied Mathematics and Physics* (2), 323-334.

Zhang, H., H. F. Wang, Q. B. Yu, Y. F. Zheng, G. C. Lu and C. Ge (2021). Perforation of double-spaced aluminum plates by reactive projectiles with different densities. *Materials* 14(5).